

Nuclear viscosity estimated by dynamics of neck formation in the early stage of nuclear collision

S. Amano¹, Y. Aritomo¹, M.Ohta²

¹Kindai University Higashi-Osaka, Osaka 577-8502, Japan

²Konan University Kobe, Hyogo 658-8501, Japan

e-mail: amano.shota3@gmail.com

Abstract

The very early stage of the coalescence of two nuclei is studied and used to estimate the nuclear viscosity. The time evolution of the neck region has been simulated by the unified Langevin equation method, which is used in the analysis of heavy-ion collisions from the approaching stage to the fusion-fission stage. It is found that the transition from viscous to inertial coalescence that appeared in the neck growth of macroscopic drops can also be seen in the present simulation in nucleus–nucleus collisions. The dynamics of neck growth is analyzed in terms of the hydrodynamical formula and the viscosity coefficient of nuclear matter is estimated using the analogy of macroscopic drops.

1 Introduction

The coalescence and rupture of liquid drops that we usually encounter in natural phenomena have been attracting considerable attention. Studies to elucidate these phenomena have a long history in the hydrodynamical field, starting from the 19th century.¹ Since then, the knowledge on the coalescence and rupture of drops has been applied to industrial devices. The nature of liquid drops is also extensively investigated in the field of microscopic matters such as nuclei. In nuclear physics, the liquid drop model has been widely used to predict the nature of nuclei composed of nucleons. Some examples are Weizsäcker’s mass formula^{2,3} and the transient state method by Bohr–Wheeler⁴ for the prediction of fission. These are part of the foundation of present-day nuclear physics.

In recent hydrodynamical studies, the mechanism of neck formation in the early stage of the coalescence of macroscopic drops has been elucidated extensively with the recent development of experimental technologies.^{5–7} These studies have shown that in a short time duration after contact, viscous forces are expected to dominate the flow of the neck region, and the neck radius evolves in proportion to time t from neck opening, but after that, in the inviscid limit, the neck radius increases in proportion to $t^{1/2}$ owing to the effect of the motion which is dominated by an inertial capillary force. The crossover point between two regions is clearly identified and studied quantitatively.^{6,7}

The dynamical properties of a growing neck in nuclear collisions have been investigated in terms of the mass parameter for the neck degree of freedom,⁸ and presented the difference of the neck formation by the microscopic mass parameter and the macroscopic Werner-Wheeler one.^{8,17} We use here the macroscopic mass parameter and study the process of neck formation just after contact.

One of the aims of the present study is to investigate how neck formation proceeds in very early stage of the collision, and to confirm that the viscous-inertial transition appearing in macroscopic drop also occurs in microscopic drops such as nuclei. At the same time, the viscosity of the nucleus is estimated from the evolution of neck formation. Thus far, the viscosity of the nucleus has been determined from experimental data in the giant dipole resonance (GDR),^{9–13} and its value is scattered around 0.025 TP (1 TP = 10^{12} P = 6.24×10^{-22} MeV s/fm³). P (poise) is the unit of viscosity. In relation to fission phenomena such as the total kinetic energy of fission fragments, fusion cross sections, and pre-neutron emission multiplicity, various values of viscosity are required for fitting experiments.¹⁴ In the analysis of fission processes, the viscosity is shown to be in the range of 0.04 TP–0.08 TP by comparing the microscopic and macroscopic dissipation energies.^{15,16} The strong viscosity is inferred from the fission transition time.¹⁷

In the recent theoretical analysis^{18,19} of the deep inelastic collision (DIC), the quasifission (QF) and the fusion-fission (FF) processes, the viscosity or the friction force is treated in general as a model parameter. To clarify the uncertainty of the viscosity or the friction force, in connection with the analysis of QF processes, we investigated the nuclear viscosity in relation with the dynamics of neck formation in the contact stage of nucleus–nucleus collisions. We show that our results are consistent with the viscosity coefficient derived from GDR experiments.

In the following sections, a brief review of the method of our Langevin calculation used in this analysis formation in the early stage of collision is investigated in comparison with the case of macroscopic drops. The derivation of nuclear viscosity coefficient is also discussed.

2 Theoretical framework

2.1 Potential energy

Since the early stage of neck formation in nucleus–nucleus collisions cannot be seen directly like macroscopic drops can be, we use the simulation by the Langevin equation method^{18,20,21} where the shape evolution of colliding nuclei is calculated in three–dimensional (3D) deformation space. In our Langevin method, the calculation begins with the separate configuration of two colliding nuclei. Then, two nuclei come into contact with each other to form a neck toward QF and FF. Therefore, for the potential energy in the 3D space, we consider the time evolution of the potential energy from the diabatic one V_{diab} to the adiabatic one V_{adiab} . The diabatic potential is calculated by a folding procedure using effective nucleon–nucleon interaction.^{18,20,22} However, the adiabatic potential energy of the system is calculated using an extended two-center shell model.²² Then, we connect the diabatic and

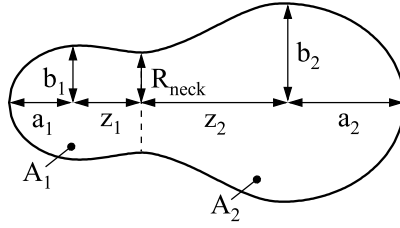


Figure 1: Example of the nuclear shape described in the two-center shell model.

adiabatic potential energies with a time-dependent weighting function $f(t)$ as

$$V(q, t) = V_{\text{diab}}(q) f(t) + V_{\text{adiab}}(q, t, L, T) [1 - f(t)], \quad (1)$$

$$f(t) = \exp\left(-\frac{t}{\tau}\right). \quad (2)$$

Here, q denotes a set of collective coordinates representing a nuclear shape. t is the interaction time and τ is the relaxation time in the transition from the diabatic potential energy to the adiabatic one. L and T denote the total angular momentum and the temperature of the compound nucleus calculated from the intrinsic energy of the composite system. We use the relaxation time $\tau = 0.1$ zs proposed in Refs.^{23–25} We use the two-center parameterizations as coordinates to represent nuclear deformation.^{26,27} To solve the dynamical equation numerically and avoid the huge computation time, we strictly limited the number of degrees of freedom and employed three parameters as follows: $z_0 = |z_1| + |z_2|$ (distance between the centers of two potentials), δ (deformation of fragment), and α (mass asymmetry of colliding nuclei); $\alpha = \frac{A_2 - A_1}{A_{\text{CN}}}$, where A_1 and A_2 not only stand for the mass numbers of the projectile and target, respectively,^{18,21} but also are then used to indicate the mass numbers of the two fission fragments. A_{CN} is the mass number of the compound nucleus. Figure 1 is the example of the nuclear shape described with the two-center parametrization. The parameter δ is defined as $\delta = \frac{3(a-b)}{2a+b}$, where a and b represent the half length of the ellipse axes in the z_0 and orthogonal to z_0 directions, respectively. We assume that each fragment has the same deformation in the first step. In addition, we use scaling to minimize the computation time and use the coordinate z defined as $z = \frac{z_0}{R_{\text{CN}}B}$, where R_{CN} denotes the radius of the spherical compound nucleus and the parameter B is defined as $B = \frac{3+\delta}{3-2\delta}$. The adiabatic potential energy is defined as

$$V_{\text{adiab}}(q, t, L, T) = V_{\text{LDM}}(q, t) + V_{\text{SH}}(q, T) + V_{\text{rot}}(q, L), \quad (3)$$

where V_{LDM} and V_{SH} are the potential energy of the finite-range liquid drop model and the microscopic energy that takes into account the temperature dependence, respectively. There is the neck parameter ϵ which is one of the parameter representing the nuclear shape. The two harmonic oscillator potentials associated with the nuclear shape are smoothly connected by the neck parameter at the $z = 0$ (See Fig. 2). Toward the smaller value of ϵ , the neck region is extended. The neck parameter is defined as

$$\epsilon = E/E_0. \quad (4)$$

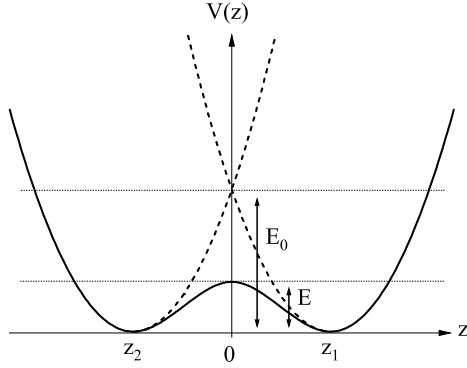


Figure 2: Two harmonic oscillator potentials corresponding the nuclear shape. Two harmonic oscillator potentials are smoothly connected by the neck parameter $\epsilon = E/E_0$.

Concerning the adiabatic potential energy calculated using the two-center shell model, the neck parameter ϵ is included in the two-center parametrization. The value of the neck parameter ϵ is recommended as 0.35 for fission processes.²⁸ In our study, we treat $\epsilon = 1$ as the entrance channel and $\epsilon = 0.35$ as the exit channel, and we assume the time dependence of ϵ to be,

$$V_{\text{LDM}}(q, t) = V_{\text{LDM}}^{\epsilon=1}(q) f_{\epsilon}(t) + V_{\text{LDM}}^{\epsilon=0.35}(q) [1 - f_{\epsilon}(t)], \quad (5)$$

$$f_{\epsilon}(t) = \frac{1}{1 + \exp\left(\frac{t-t_0}{\Delta_{\epsilon}}\right)}. \quad (6)$$

The temporal form of ϵ has been used commonly^{22,29-31} and we adopted the characteristic relaxation time of the neck $t_0 = 0.35$ zs and the variance $\Delta_{\epsilon} = 0.1$ zs in the present study.

In the two-center parametrization, the neck radius R_{neck} is calculated from

$$R_{\text{neck}} = \sqrt{\frac{b_1^2 - \left(\frac{z_1}{B}\right)^2 \epsilon}{1 + G1}} \approx \sqrt{\frac{b_1^2 - \left(\frac{z_2}{B}\right)^2 \epsilon}{1 + G2}}, \quad (7)$$

$$G1 = \frac{z_1}{z_2 - z_1} \left[1 - \left(\frac{b_2}{b_1}\right)^2 \right], \quad G2 = -\frac{z_2}{z_2 - z_1} \left[1 - \left(\frac{b_1}{b_2}\right)^2 \right]. \quad (8)$$

The simplified symbol V_{LDM} and the symbol V_{SH} are described as

$$V_{\text{LDM}}(q) = E_{\text{S}}(q) + E_{\text{C}}(q), \quad (9)$$

$$V_{\text{SH}}(q, T) = E_{\text{shell}}^0(q) \Phi(T), \quad (10)$$

$$E_{\text{shell}}^0(q) = \Delta E_{\text{shell}}(q) + \Delta E_{\text{pair}}(q). \quad (11)$$

The symbols E_{S} and E_{C} stand for generalized surface energy³² and Coulomb energy, respectively. The symbol E_{shell}^0 indicates the microscopic energy at $T = 0$, which is calculated as the sum of the shell correction energy ΔE_{shell} and the pairing correlation correction energy ΔE_{pair} . ΔE_{shell} is calculated by the Strutinsky method^{33,34} from the single-particle levels of the two-center shell model potential^{26,35,36} as the difference between the sum of single-particle energies of occupied states and the

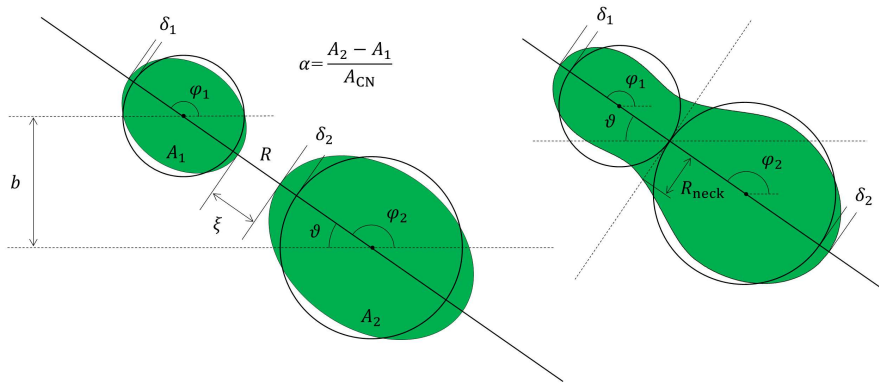


Figure 3: Geometrical diagram with degrees of freedom used in the model.

averaged quantity. ΔE_{pair} is evaluated in the BCS approximation as described in Refs.^{34,37} The averaged part of the pairing correlation energy is calculated assuming that the density of single-particle states is constant over the pairing window. The pairing strength constant is related to the average gap parameter $\tilde{\Delta}$ by solving the gap equation in the same approximation and adopting $\tilde{\Delta} = 12/\sqrt{A}$ suggested in³⁷ by considering the empirical results for the odd-even mass difference.³⁸ The temperature dependence factor $\Phi(T) = \exp\left(-\frac{E^*}{E_d}\right)$ is explained in Ref.,²¹ where E^* indicates the excitation energy of the compound nucleus. E^* is given as $E^* = aT^2$, where a is the level density parameter. The shell damping energy E_d is selected as 20 MeV. This value is given by Ignatyuk et al.³⁹ V_{rot} is the centrifugal energy generated from the total angular momentum L . We obtain

$$V_{\text{rot}}(q, L) = \frac{\hbar^2 \ell(\ell + 1)}{2\mathcal{I}(q)} + \frac{\hbar^2 L_1(L_1 + 1)}{2\mathfrak{S}_1(q)} + \frac{\hbar^2 L_2(L_2 + 1)}{2\mathfrak{S}_2(q)}. \quad (12)$$

Here, $\mathcal{I}(q)$ and ℓ represent the moment of inertia of the rigid body with deformation q and the relative orientation of nuclei and relative angular momentum respectively. The moment of inertia and the angular momentum for the heavy and light fragments are $\mathfrak{S}_{1,2}$ and $L_{1,2}$, respectively.

2.2 Langevin equation

Langevin-type equations have seven degrees of freedom $\{R, \delta_1, \delta_2, \alpha, \vartheta, \varphi_1, \varphi_2\}$ as shown schematically in Fig. 3. However, in the present paper we set $\delta_1 = \delta_2$. We perform trajectory calculations of the time-dependent unified potential energy^{18,20,21}

using the multidimensional Langevin equation^{18,21,40} as follows :

$$\begin{aligned}
\frac{dq_i}{dt} &= (m^{-1})_{ij} p_j, \\
\frac{dp_i}{dt} &= -\frac{\partial V}{\partial q_i} - \frac{1}{2} \frac{\partial}{\partial q_i} (m^{-1})_{jk} p_j p_k - \gamma_{ij} (m^{-1})_{jk} p_k + g_{ij} \Gamma_j(t), \\
\frac{d\vartheta}{dt} &= \frac{\ell}{\mu_R R^2}, \quad \frac{d\varphi_1}{dt} = \frac{L_1}{\mathfrak{S}_1}, \quad \frac{d\varphi_2}{dt} = \frac{L_2}{\mathfrak{S}_2}, \\
\frac{d\ell}{dt} &= -\frac{\partial V}{\partial \vartheta} - \gamma_{\text{tan}} \left(\frac{\ell}{\mu_R R^2} - \frac{L_1}{\mathfrak{S}_1} a_1 - \frac{L_2}{\mathfrak{S}_2} a_2 \right) R + R \sqrt{\gamma_{\text{tan}} T} \Gamma_{\text{tan}}(t), \\
\frac{dL_1}{dt} &= -\frac{\partial V}{\partial \varphi_1} + \gamma_{\text{tan}} \left(\frac{\ell}{\mu_R R^2} - \frac{L_1}{\mathfrak{S}_1} a_1 - \frac{L_2}{\mathfrak{S}_2} a_2 \right) a_1 - a_1 \sqrt{\gamma_{\text{tan}} T} \Gamma_{\text{tan}}(t), \\
\frac{dL_2}{dt} &= -\frac{\partial V}{\partial \varphi_2} + \gamma_{\text{tan}} \left(\frac{\ell}{\mu_R R^2} - \frac{L_1}{\mathfrak{S}_1} a_1 - \frac{L_2}{\mathfrak{S}_2} a_2 \right) a_2 - a_2 \sqrt{\gamma_{\text{tan}} T} \Gamma_{\text{tan}}(t). \quad (13)
\end{aligned}$$

The collective coordinates q_i represent z , δ , and α , the symbol p_i denotes momentum conjugated to q_i , and V is the multidimensional potential energy. The symbol ϑ indicates the relative orientation of nuclei. φ_1 and φ_2 stand for the rotation angles of the nuclei in the reaction plane, $a_{1,2} = \frac{R}{2} \pm \frac{R_1 - R_2}{2}$ is the distance from the center of the fragment to the middle point between the nuclear surfaces, and $R_{1,2}$ is the nuclear radii. The symbol R is the distance between the nuclear centers. The total angular momentum $L = \ell + L_1 + L_2$ is preserved.

The symbol μ_R is reduced mass, and γ_{tan} is the tangential friction force of the colliding nuclei. Here, it is called sliding friction. The phenomenological nuclear friction forces for separated nuclei are expressed in terms of γ_{tan} and γ_R for sliding friction and radial friction using the Woods-Saxon radial form factor described in Ref.¹⁸ Sliding and radial friction are described as $\gamma_{\text{tan}} = \gamma_t^0 F(\xi)$ and $\gamma_R = \gamma_R^0 F(\xi)$, where the radial form factor $F(\xi) = \left(1 + \exp^{\frac{\xi - \rho_F}{a_F}} \right)^{-1}$. γ_t^0 and γ_R^0 being the model parameters employed 0.1×10^{-22} MeV s fm⁻² and 100×10^{-22} MeV s fm⁻², respectively. $\rho_F \approx 2$ fm and $a_F \approx 0.6$ fm are also the model parameters determined in Ref.¹⁸ and ξ is the distance between the nuclear surfaces $\xi = R - R_{\text{contact}}$, where $R_{\text{contact}} = R_1 + R_2$.¹⁸ The phenomenological friction for the radial direction is switched to the one-body friction in the mononucleus stage. γ_R is described to consider the kinetic dissipation according to the surface friction model⁴¹ The radial friction is calculated as $\gamma_{zz} = \gamma_{zz}^{\text{one}} + \Omega(\xi) \gamma_R$. For the mononuclear system, the wall-and-window one-body dissipation γ_{zz}^{one} is adopted for the friction tensor.^{14,42-48} $\Omega(\xi)$ is smoothing function switched the phenomenological friction to that of a mononuclear system as follows $\Omega(\xi) = \left(1 + \exp^{-\frac{\xi}{0.3}} \right)^{-1}$.¹⁸ m_{ij} and γ_{ij} stand for the shape-dependent collective inertia and friction tensors, respectively. We adopted the hydrodynamical inertia tensor m_{ij} in the Werner-Wheeler approximation for the velocity field.¹⁷ The one-body friction tensors γ_{ij} are evaluated within the wall-and-window formula.^{44,49} The normalized random force $\Gamma_i(t)$ is assumed to be white noise: $\langle \Gamma_i(t) \rangle = 0$ and $\langle \Gamma_i(t_1) \Gamma_j(t_2) \rangle = 2\delta_{ij} \delta(t_1 - t_2)$. According to the Einstein relation, the strength of the random force g_{ij} is given as $\gamma_{ij} T = \sum_k g_{ik} g_{jk}$.

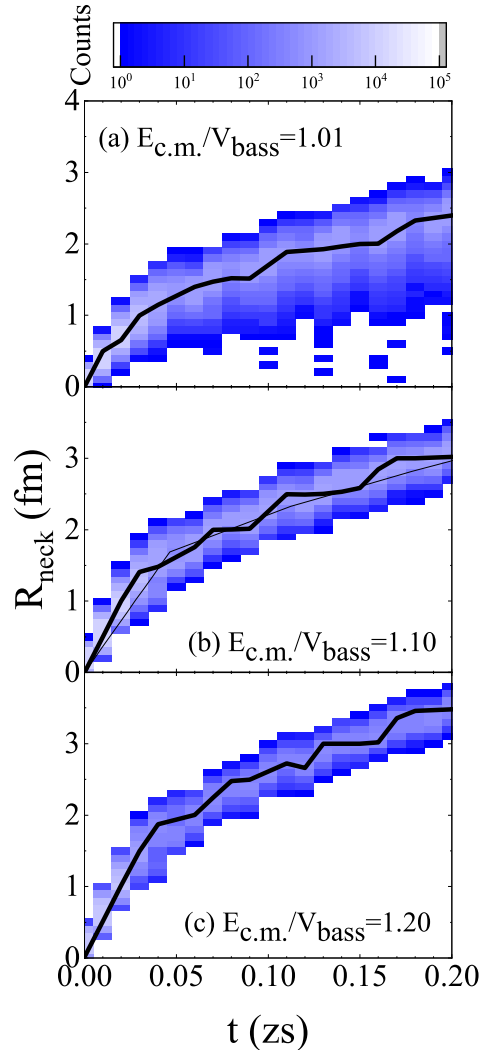


Figure 4: Two-dimensional R_{neck} -time matrices for the $^{136}\text{Xe} + ^{136}\text{Xe}$ reaction at $E_{\text{c.m.}}/V_{\text{bass}} =$ (a) 1.01, (b) 1.10, and (c) 1.20. The black lines are the ridges of the contour map. The thin line is the calculation result of the neck radius with no fluctuation. The neck radii at each time step in 20000 calculations are accumulated to make contour maps.

3 Results and discussion

3.1 Neck growth in the early stage

To analyze the dynamics of neck formation at the early stage of heavy-ion collisions, the fluctuation of the neck radius R_{neck} versus evolution time for the $^{136}\text{Xe} + ^{136}\text{Xe}$ reaction is calculated. The calculations are performed at different centers of mass incident energies; $E_{\text{c.m.}}/V_{\text{bass}} = 1.01, 1.10,$ and 1.20 are calculated and are shown in Fig. 4, where V_{bass} means the Bass barrier energy $V_{\text{bass}} = 299.56$ MeV.⁵⁰ The neck radius is extracted from each time step of the calculation and overplotted for 20000 trials. The values of neck radius are distributed as drawn by the contour map in Fig. 4, and the ridges are shown by the black lines. The presentations of calculations are restricted to the early stage of collision up to 0.2 zs. The rate of growth of the neck radius decreases beyond $t \approx 0.01, 0.03,$ and 0.04 zs for $E_{\text{c.m.}}/V_{\text{bass}} = 1.01, 1.10,$ and

1.20, respectively. Here, we define the region where the neck grows linearly as the viscous regime and the region thereafter as the inertial regime.

It is noted that in order to check the similarity with the neck formation of the macroscopic coalescence of water drop at first, the orbital angular momentum is set to zero in the nuclear collision system. When we estimate the viscosity in the later section, the finite value of angular momentum corresponding to QF or DIC phenomena are used in the calculation.

In Fig. 4(a), the distribution spreads widely to the lower part because of the rapid disappearance of the neck owing to increasing components of DIC with decreasing incident energy. The thin line in Fig. 4(b) represents the result with no fluctuation. Without fluctuation, the neck radius is uniquely determined. As can be seen in the black lines in Figs. 4(a)–(c), R_{neck} s grow linearly up to 0.01, 0.03, and 0.04 zs for each incident energy. This dependence on $E_{\text{c.m.}}$ is due to the extra kinetic energy of the projectile after contact. The relative velocities of two colliding nuclei are 29, 31, and 32 fm/zs, corresponding to three incident energies. On the other hand, the growth rate of R_{neck} decreases in the inertial regime. The change in this slope signifies the transition of dynamics, as thoroughly discussed in studies of water drops.^{5–7, 51–55} Here, the neck radius is estimated from the dam-bell shape of stuck nuclei.

We confirmed that these characteristics of neck formation in the very early stage can be seen even for the parameters t_0 and Δ_ϵ of temporal function changing in the range $0.1 \text{ zs} \leq t_0 \leq 1 \text{ zs}$ and $0.1 \text{ zs} \leq \Delta_\epsilon \leq 10 \text{ zs}$.

3.2 Viscous-inertial crossover

In the viscous regime, the capillary forces drive the growth of the neck against the viscosity. The function of the neck radius with respect to time t , $R_{\text{neck}}(t) \approx C_0 \sigma t / \eta$ can be driven from the understanding that the decreased amount in the surface energy is dissipated by the viscosity.^{7, 52, 57} The value of the coefficient C_0 is 1.5 ($= 3/2$) in this study. Here, σ shows the surface tension per unit area and the conventional value is used. η denotes the viscosity of the nuclear matter.

On the other hand, when sufficient time elapses, the decrease in the surface energy is converted to the kinetic energy which corresponds to the beginning of the motion of the nucleons in the neck region. Considering the balance of the kinetic energy with the surface energy, the neck radius is expressed as $R_{\text{neck}}(t) \approx D_0 (\sigma R_0 / \rho)^{1/4} \sqrt{t}$ ^{56, 57} in the inertial regime. $R_0 = 1.2A^{1/3}$ represents the nuclear radius with mass number A before the collisions. ρ is the nucleus density and is assumed to be $2.5 \times 10^{17} \text{ kg/m}^3$. The value of the coefficient D_0 is approximately 1.19 ($\sim 2^{1/4}$) in our study. The values of both C_0 and D_0 are on the order of 1. These values are also reasonable for the analysis in our results, as reported in Refs.^{6, 7, 56}

These two functions for neck are plotted in Fig. 5 with the calculation results indicated by the black lines in Fig. 4. We resize the coordinate scales in Fig. 5 to focus on the transition of the dynamics. From the data of linear dependence on time in the viscous regime in Fig. 5, we can extract the viscosity coefficient. The linear dependence of neck radius on time is drawn by the green solid line using the optimum value of η . The values of the viscosity coefficient extracted from Figs. 5(a), 5(b), and 5(c) are 0.0092 TP, 0.0090 TP, and 0.0086 TP, respectively.

In the collisions of superheavy nuclei, an inner barrier exists even after overcom-

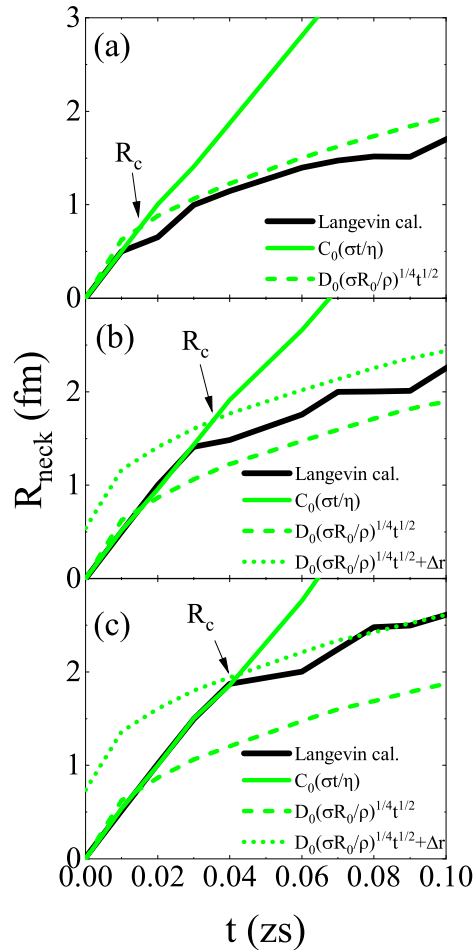


Figure 5: Neck radius R_{neck} during coalescence as a function of the time elapsed from the first connected neck for the $^{136}\text{Xe} + ^{136}\text{Xe}$ reaction at $E_{\text{c.m.}}/V_{\text{bass}} =$ (a) 1.01, (b) 1.10 and (c) 1.20. The solid black lines are the same as shown in Fig. 4. The green solid and dashed lines signify viscous-capillary ($R_{\text{neck}} \propto t$) and inertial-capillary scaling ($R_{\text{neck}} \propto t^{1/2}$). The dotted lines are the function of R_{neck} considering the flow dynamics of the interacting region in nucleus–nucleus collisions. The correction factor Δr and the coefficients C_0 and D_0 are explained in the text. The arrows indicate the crossover point R_c .

ing the Coulomb barrier. In the case of high-incident-energy reactions as in Figs. 5(b) and 5(c), because of the incompressibility of nuclear matter, the compressive area thought to arise owing to the interaction with the inner barrier is evaded. Instead, the neck radius is considered to enlarge without changing the neck width. This effect is taken into account by the additional parameter Δr . In the experiment of the coalescence of droplets,^{5–7,51,52,54,55} the relative velocity between them is considered to be zero. In contrast, in our reaction system, the relative velocity of colliding nuclei is inevitable to overcome the Coulomb barrier for the coalescence. In this point, for the present case the dominant motion in the neck region is different from the macroscopic case⁵⁶ in the viscous regime. This is the reason why the parameter Δr is introduced above.

The crossover point R_c has energy dependence, and the values are 0.6 fm, 1.6 fm, and 1.87 fm in Figs. 5(a)–(c), respectively. From the corresponding shift of $R_{\text{neck}}(t)$

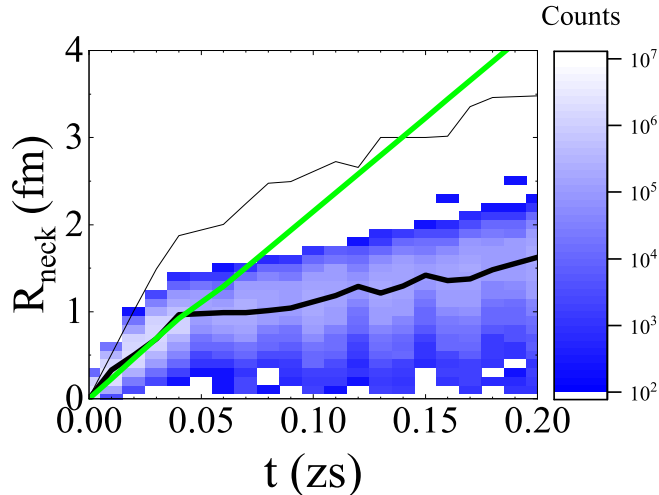


Figure 6: Two-dimensional R_{neck} -time matrices for $L = 210\hbar$ in the reaction of $^{136}\text{Xe} + ^{136}\text{Xe}$ at $E_{\text{c.m.}}/V_{\text{bass}} = 1.20$. The thick black line is the ridges of the contour map. The neck radii at each time step in 900000 calculations are accumulated to make contour maps. The thin black line is the same as the result shown in Fig. 4(c). The green line signifies viscous-capillary ($R_{\text{neck}} \propto t$) scaling using $R_{\text{neck}}(t) \approx C_0\sigma t/\eta$.

in the inertial regime, the values of Δr for the case of Figs. 5(b) and 5(c) are 0.54 and 0.74 fm.

3.3 Viscosity coefficient for the case with large impact parameter

We have carried out a new method to estimate the nuclear viscosity coefficient from the neck formation. In order to compare the viscosity coefficients from experimental data in the GDR, the calculations are performed for high orbital angular momentum ($L = 210\hbar$). Figure 6 shows two-dimensional R_{neck} -time matrices for $L = 210\hbar$ in the reaction of $^{136}\text{Xe} + ^{136}\text{Xe}$ at $E_{\text{c.m.}}/V_{\text{bass}} = 1.20$. The distribution spreads widely to the lower part because of the rapid disappearance of the neck owing to increasing component of DIC comparing the result in Fig. 4(c). The thin black line is the same as the black line in Fig. 4(c) calculated with $L = 0\hbar$. At high orbital angular momentum, the rapid growth of the neck appearing in the viscous regime is suppressed and the slope is gentle due to less effect from the compressive region. The change in neck radius is represented by the green line using the equation: $R_{\text{neck}}(t) \approx C_0\sigma t/\eta$. When we fit the green line to the slope from 0 zs to 0.04 zs indicated by the thick black line, we obtain $\eta = 0.02 \pm 0.01$ TP. Next, we evaluate the value of the viscosity coefficient estimated using the friction tensor $\gamma_{\alpha\alpha}$ and the inertia tensor $m_{\alpha\alpha}$ treated in our model. The kinematic viscosity coefficient ν is shown using reduced friction coefficient $\beta_{\alpha\alpha}(q)$ as follows⁵⁸⁻⁶⁰

$$\beta_{\alpha\alpha}(q) = \frac{\gamma_{\alpha\alpha}}{m_{\alpha\alpha}}, \quad (14)$$

$$\nu = \frac{\beta_{\alpha\alpha}(q) R_{\text{neck}}^2}{6}, \quad (15)$$

η treated as a two-body viscosity coefficient in nuclear physics is obtained using kinematic viscosity coefficient as $\eta = \rho\nu$. Averaging the values of η between 0 zs and 0.04 zs where the viscous-capillary force is dominant, $\eta \approx 0.021$ TP is obtained in the present case. The viscosity coefficient obtained from the reduced friction coefficient is almost consistent with the one obtained from the slope of the neck formation in our Langevin calculation.

4 Conclusion

The dynamics of the growing neck radius in nucleus–nucleus collisions has been investigated by the unified Langevin equation method assuming the macroscopic mass parameter. We have chosen the $^{136}\text{Xe} + ^{136}\text{Xe}$ system as an example and focused on the early stage of collision, where the nuclear viscosity clearly controls the neck formation. The values of the viscosity coefficient of the nucleus extracted in this study have been found to be $\eta = 0.02 \pm 0.01$ TP, which is comparable to the viscosity determined from experimental data in GDR. It is noted that the change in the dynamics occurred in the coalescence of nuclei is similar to the case of water drops. The viscous-capillary force ($R_{\text{neck}} \propto t$) works at short times, and the inertial-capillary force ($R_{\text{neck}} \propto t^{1/2}$) is dominant at later stage. It is remarkable that even in microscopic drops such as nuclei, the viscous-inertial crossover can be seen in the present simulation independent of the temporal form of neck parameter ϵ .

Acknowledgments

The Langevin calculation was performed using the cluster computer system (Kindai-VOSTOK) under the supported of JSPS KAKENHI Grant Number 20K04003 and Research funds for External Fund Introduction 2021 provided by Kindai University.

References

- [1] T. J. John and N. H. Frank, *Proc. R. Soc. Lond* **39**, 239 (1886).
- [2] C. F. v. Weizsäcker, *Z. Physik* **96**, 431 (1935).
- [3] H. A. Bethe and R. F. Bacher, *Rev. Mod. Phys.* **8**, 82 (1936).
- [4] N. Bohr and J. A. Wheeler, *Phys. Rev.* **56**, 426 (1939).
- [5] D. G. A. L. Aarts, H. N. W. Lekkerkerker, H. Guo, G. H. Wegdam, and D. Bonn, *Phys. Rev. Lett.* **95**, 164503 (2005).
- [6] J. C. Burton and P. Taborek, *Phys. Rev. Lett.* **98**, 224502 (2007).
- [7] J. D. Paulsen, J. C. Burton, and S. R. Nagel, *Phys. Rev. Lett.* **106**, 114501 (2011).
- [8] G.G.Adamian, N.V.Antonenko, A.Diaz-Torres, W.Scheid, *Nucl. Phys. A* **671**, 233-254 (2000).

- [9] G. Enders, F. D. Berg, K. Hagel, W. Kühn, V. Metag, R. Novotny, M. Pfeiffer, O. Schwalb, R. J. Charity, A. Gobbi, R. Freifelder, W. Henning, K. D. Hildenbrand, R. Holzmann, R. S. Mayer, R. S. Simon, J. P. Wessels, G. Casini, A. Olmi, and A. A. Stefanini, *Phys. Rev. Lett.* **69**, 249 (1992).
- [10] T. Baumann, E. Ramakrishnan, A. Azhari, J. Beene, R. Charity, J. Dempsey, M. Halbert, P.-F. Hua, R. Kryger, P. Mueller, R. Pfaff, D. Sarantites, L. Sobotka, D. Stracener, M. Thoennessen, G. Van Buren, R. Varner, and S. Yokoyama, *Nuclear Physics A* **635**, 428 (1998).
- [11] M. P. Kelly, K. A. Snover, J. P. S. van Schagen, M. Kicińska-Habior, and Z. Trznadel, *Phys. Rev. Lett.* **82**, 3404 (1999).
- [12] P. Heckman, D. Bazin, J. Beene, Y. Blumenfeld, M. Chromik, M. Halbert, F. Liang, E. Mohrmann, T. Nakamura, A. Navin, B. Sherrill, K. Snover, *Physics Letters B* **555**, 43 (2003).
- [13] N. Auerbach and S. Shlomo, *Phys. Rev. Lett.* **103**, 172501 (2009).
- [14] T. Wada, Y. Abe, and N. Carjan, *Phys. Rev. Lett.* **70**, 3538 (1993).
- [15] S. Koonin, R. Hatch, and J. Randrup, *Nuclear Physics A* **283**, 87 (1977).
- [16] A. J. Sierk, S. E. Koonin, and J. R. Nix, , *Phys. Rev. C* **17**, 646 (1978).
- [17] K. T. R. Davies, A. J. Sierk, and J. R. Nix, *Phys. Rev. C* **13**, 2385 (1976).
- [18] V. Zagrebaev and W. Greiner, *Journal of Physics G: Nuclear and Particle Physics* **31**, 825 (2005).
- [19] S. Amano, Y. Aritomo, and M. Ohta, *Phys. Rev. C* **106**, 024610 (2022).
- [20] V. Zagrebaev and W. Greiner, *Journal of Physics G: Nuclear and Particle Physics* **34**, 2265 (2007).
- [21] Y. Aritomo and M. Ohta, *Nuclear Physics A* **744**, 3 (2004).
- [22] V. Zagrebaev, A. Karpov, Y. Aritomo, M. Naumenko, and W. Greiner, *Physics of Particles and Nuclei* **38**, 469 (2007).
- [23] G. Bertsch, *Zeitschrift für Physik A Atoms and Nuclei* **289**, 103 (1978).
- [24] W. Cassing and W. Nörenberg, *Nuclear Physics A* **401**, 467 (1983).
- [25] A. Diaz-Torres, *Phys. Rev. C* **69**, 021603(R) (2004).
- [26] J. Maruhn and W. Greiner, *Zeitschrift für Physik* **251**, 431 (1972).
- [27] K. Sato *et al.*, *Zeitschrift für Physik A Atoms and Nuclei* **288**, 383 (1978).
- [28] S. Yamaji, H. Hofmann, and R. Samhammer, *Nuclear Physics A* **475**, 487 (1987).
- [29] V. Saiko and A. Karpov, *Eur. Phys. J. A* (2022) **58**, 41 (2022).

- [30] V. V. Saiko and A. V. Karpov, *Phys. Rev. C* **99**, 014613 (2019).
- [31] A. V. Karpov and V. V. Saiko, *Phys. Rev. C* **96**, 024618 (2017).
- [32] H. J. Krappe, J. R. Nix, and A. J. Sierk, *Phys. Rev. C* **20**, 992 (1979).
- [33] V. Strutinsky, *Nuclear Physics A* **122**, 1 (1968).
- [34] M. Brack *et al.*, *Rev. Mod. Phys.* **44**, 320 (1972).
- [35] S. Suekane, A. Iwamoto, S. Yamaji, and K. Harada, JAERI-memo, 5918 (1993).
- [36] A. Iwamoto *et al.*, *Progress of Theoretical Physics* **55**, 115 (1976).
- [37] S. G. Nilsson *et al.*, *Nuclear Physics A* **131**, 1 (1969).
- [38] Y. Aritomo, S. Chiba, and F. Ivanyuk, *Phys. Rev. C* **90**, 054609 (2014).
- [39] A. Ignatyuk, G. Smirenkin, and A. Tishin, *Yadernaya Fizika* **21**, 485 (1975).
- [40] Y. Aritomo, *Phys. Rev. C* **80**, 064604 (2009).
- [41] P. Fröbrich and I. I. Gontchar, *Physics Reports* **292**, 131 (1998).
- [42] J. Blocki *et al.*, *Annals of Physics* **113**, 330 (1978).
- [43] J. R. Nix and A. J. Sierk, *Nuclear Physics A* **428**, 161 (1984).
- [44] J. Randrup and W. Swiatecki, *Nuclear Physics A* **429**, 105 (1984).
- [45] H. Feldmeier, *Reports on Progress in Physics* **50**, 915 (1987).
- [46] N. Cârjan, A. J. Sierk, and J. R. Nix, *Nuclear Physics A* **452**, 381 (1986).
- [47] N. Cârjan, T. Wada, and Y. Abe, AIP Conference Proceedings (1992).
- [48] T. Asano *et al.*, *Journal of Nuclear and Radiochemical Sciences* **7**, 7 (2006).
- [49] A. J. Sierk and J. R. Nix, *Phys. Rev. C* **21**, 982 (1980).
- [50] R. Bass, Nuclear reactions with heavy ions (1980).
- [51] X. Xia, C. He, and P. Zhang, *Proceedings of the National Academy of Sciences* **116**, 23467 (2019).
- [52] M. Yokota and K. Okumura, *Proceedings of the National Academy of Sciences* **108**, 6395 (2011).
- [53] V. Akella and H. Gidituri, *Chemical Physics Letters* **758**, 137917 (2020).
- [54] S. T. THORODDSEN, K. TAKEHARA, and T. G. ETOH, *Journal of Fluid Mechanics* **527**, 85–114 (2005).
- [55] J. Paulsen, R. Carmigniani, A. Kannan, J. Burton, and S. Nagel, *Nature communications* **5**, 3182 (2014).

- [56] L. DUCHEMIN, J. EGGERS, and C. JOSSERAND, *Journal of Fluid Mechanics* **487**, 167–178 (2003).
- [57] J. EGGERS, J. R. LISTER, and H. A. STONE, *Journal of Fluid Mechanics* **401**, 293–310 (1999).
- [58] A. V. Karpov and G. D. Adeev, *Phys. At. Nucl.* **65**, 1596 (2002).
- [59] E. S. Hernandez, W. D. Myers, J. Randrup, and B. Remaud, *Nucl. Phys. A* **361**, 483 (1981).
- [60] G. D. Adeev, A. V. Karpov, P. N. Nadtochii, and D. V. Vanin, *Physics of Particles and Nuclei* **36(4)** **401**, 378–426 (2005).